A review of 9-year performance and operation of the MOPITT instrument

James R. Drummond [a,b], Jiansheng Zou [a,*], Florian Nichitiu [a], Jayanta Kar [a,1],
Robert Deschambaut [c], John Hackett [c]

[a] *Department of Physics, University of Toronto, 60 St. George Street, Toronto, Ont., Canada M5S 1A7*
[b] *Department of Physics and Atmospheric Science, Dalhousie University, 6310 Coburg Road, Halifax, NS, Canada B3H 3J5*
[c] *COM DEV Ltd., 155 Sheldon Drive, Cambridge, Ont., Canada N1R 7H6*

Abstract

The MOPITT (Measurements of Pollution in the Troposphere) instrument has provided more than nine years of global carbon monoxide (CO) measurements on a continuous basis since its launch aboard the Terra Spacecraft on December 18th, 1999. This paper gives an overview of the core sub-system performance and major issues of the in-flight instrument over the mission period. Some of the instrument anomalies are also discussed. The major successes are: (1) the concept of using a combination of correlation systems such as Length Modulated Cells (LMCs) and Pressure Modulated Cells (PMCs) to retrieve CO profiles in the troposphere; (2) the redundant design in the instrumentation which was crucial for coping with unexpected in-flight anomalies and for continuing the mission in the case of component failure; (3) the thermal environment on orbit that is so stable that some calibration procedures are not necessary; and (4) the recent production of CO total column retrieved from the MOPITT 2.3 μm channel.
© 2009 COSPAR. Published by Elsevier Ltd. All rights reserved.

Keywords: MOPITT; Satellite; Instrument; Operation; CO; Measurement

1. Introduction

1.1. Science mission

The MOPITT (Measurements of Pollution in the Troposphere) mission was the first space mission that targeted measurements of carbon monoxide on a continuous basis. MOPITT was launched on December 18th, 1999 and started nominal scientific measurements in March 2000. MOPITT measures upwelling radiation in three narrow infrared (IR) bands: (1) 4.7 μm channels that have strong carbon monoxide (CO) absorption characteristics and are referred to as CO thermal channels because the dominant signals are from the thermal emission of the atmosphere and the Earth's surface; (2) 2.3 μm channels that have weak CO absorption and are referred to as CO solar channels due to the reflected sunlight being the dominant signal; and (3) 2.2 μm channels that have weak methane (CH_4) absorption for the band where reflected sunlight is the major signal source and are termed the methane solar channels.

Current MOPITT public data products, available at the NASA Langley Atmospheric Science Data Center (http://eosweb.larc.nasa.gov/), are from the CO thermal channels and represent vertical profiles of CO mixing ratios in the troposphere over the mission. This is a unique data set and has been used to greatly improve our understanding of the distribution and transport of CO over the entire globe. Fig. 1 shows the monthly averaged CO map on a $1° \times 1°$ grid for May 2000. It captures the main sources of CO emission and the transport patterns around the

* Corresponding author. Tel.: +1 416 9781297; fax: +1 416 9788905.
E-mail address: jason.zou@utoronto.ca (J. Zou).
[1] Present address: Science Systems and Applications Inc., Hampton, VA, USA.
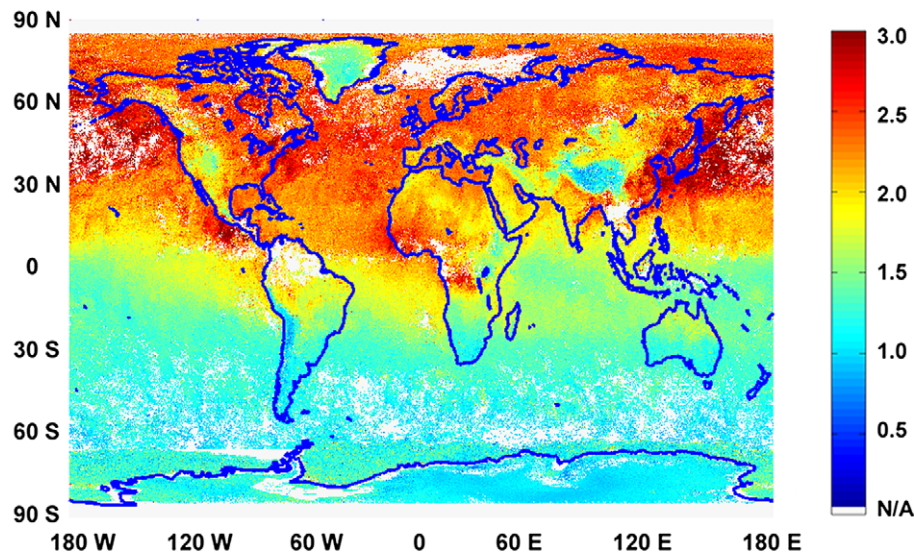
Total Column CO (10¹⁸mol cm⁻²), Monthly Mean, 2000 May

Fig. 1. Global map of monthly averaged MOPITT CO total column on a $1° \times 1°$ grid for May 2000.

globe, e.g. eastward transport over the northern Pacific that originated from southeastern Asia and the westward transport over the tropical Atlantic from Africa.

CO has become a favored target gas for space-borne measurements because of its limited lifetime of a few weeks. As such it is a useful tracer for studying pollution transport and associated atmospheric processes. Numerous studies using MOPITT CO data have been carried out including: the description of global and seasonal CO climatology and identification of major sources of CO emission (Edwards et al., 2004, 2006a); the correlation of interannual CO variations over marine continents and northern Australia with El Niño events as a dry condition favors forest fires (Edwards et al., 2006b); the observation of large horizontal gradients of CO on the synoptic scales associated with vertical and horizontal transport of air with different CO concentrations at distinctive meteorological conditions (Liu et al., 2006); a strong enhancement of upper tropospheric CO in the Asian summer monsoon region due to deep convective transport (Kar et al., 2004); enhanced CO over the Zagros mountains in Iran generated in a process of mountain venting (Kar et al., 2006); the observation of isolated CO plumes in several cities and urban areas where the CO emissions are mainly anthropogenic (Clerbaux et al., 2008). Because current MOPITT products (Version 3) are based only on thermal-channel radiances, sensitivity to CO in the boundary layer tends to be low except in regions of high thermal contrast (Deeter et al, 2007). The solar channels were not incorporated due to the high noise level of the measurements. However, a recent study on MOPITT CO solar channels has reported encouraging results in the retrieval of CO total column (Deeter et al., 2009).

A similar high noise has been seen in the methane channels of the instrument and, up to the present time, this has prevented a useful quantitative retrieval of the methane amount.

1.2. Other space instruments

There were a few missions capable of measuring CO before MOPITT. The MAPS (Measurements of Air Pollution from Satellites) was in many ways the precursor mission to MOPITT and flew on the shuttle in 1981, 1984 and 1994 (Reichle et al., 1999). Also a correlation radiometer, though of earlier design, MAPS produced similar data to MOPITT in a more restricted regime of pixel size and spatial coverage. The limited duration of the shuttle mission and conflicting operational requirements combined to limit the coverage. However the major features of the CO global distribution were shown by MAPS. The Interferometric Monitor for Greenhouse Gases (IMG) was a Japanese instrument on the ADEOS-1 mission launched in August 1996. This was a nadir pointing Fourier Transform Infrared Radiometer (FTIR) with a resolution of $0.1 \, cm^{-1}$ in the 4.7 µm band (Kobayashi et al., 1999). Unfortunately, due to a power failure of its solar panel ADEOS-1 stopped collecting data in June 1997. The Atmospheric Trace Molecules Observed by Spectroscopy (ATMOS) was a shuttle-based solar occultation Fourier Transform Spectrometer and was launched on four occasions in 1985, 1992, 1993 and 1994 (Gunson et al., 1996). Like all occultation instruments it produced high resolution vertical profiles, but was restricted in its ability to penetrate to the lower troposphere.

There are several CO missions currently on orbit. The Atmospheric Infrared Sounder (AIRS) instrument (Chahine et al., 2006) launched on the Aqua satellite in 2002 measures in the 4.7 µm band with a spectral resolution of $\sim 2 \, cm^{-1}$ and has a ground pixel size of 13.5 km at nadir.

It has a sufficient swath to offer almost daily global coverage. The Tropospheric Emission Spectrometer (TES) instrument (Beer et al., 2001) launched on the Aura satellite measures in the 4.7 μm band with a spectral resolution of ~0.06 cm^{-1} and has a ground pixel size of 0.5 × 5 km. It has no side-scan capability. The Scanning Imaging Absorption Spectrometer for Atmospheric CHartographY (SCIAMACHY) instrument (Buchwitz et al., 2004) launched on the Envisat satellite in 2002 measures in the 2.3 μm band with a spectral resolution of ~2.5 cm^{-1} and has a ground pixel size of 15 × 26 km. It provides 50% coverage of the globe on the daylight side with a swath width of 960 km. It has similar characteristics to the MOPITT CO solar channels (discussed below). Limb instruments, such as the Microwave Limb Sounder (MLS) (Froidevaux et al., 2006) launched on the Aura satellite in 2004 and the Atmospheric Chemistry Experiment (ACE) instrument (Bernath et al., 2005) launched on Canada's Scisat-1 in 2003, measure in the troposphere, but both instruments restrict their measurement to the mid-troposphere and above. The most recent satellite instrument to measure CO is the Infrared Atmospheric Sounding Interferometer (IASI), which was launched on MetOp-A in October 2006. Successive instruments will be carried on follow-on series MetOp-B and -C over a total period of 14 years. It has a wide swath of 2200 km and has a matrix field of view with 2 × 2 circular pixels of 12 km diameter. It provides daily coverage of CO "total column" (Turquety et al., 2004) similar to that of the MOPITT CO thermal channels (discussed below).

Compared to the other instruments in orbit, the gas correlation technology employed in MOPITT has its own peculiar strengths in terms of the usage of spectral information: (1) an equivalently high spectral resolution that enables retrieval of elements of the vertical profile; (2) high signal to noise ratio since many spectral lines are sampled simultaneously; (3) automatic rejection of contaminating gas signals; and (4) reduced data rate since information is essentially integrated in a radiometric, rather than spectroscopic measurement. Together these lead to an instrument with a high spatial coverage, significant vertical resolution and a modest data rate.

2. MOPITT instrument and mission profile

2.1. The Terra mission

The Terra mission is the first of a series of NASA's Earth Observing System (EOS) program, followed by the Aqua and Aura missions, for long-term monitoring of the Earth environment at the decadal time scale. Fig. 2 is a schematic of the Terra spacecraft. It flies in a sun-synchronous polar low Earth orbit (LEO) at an altitude of 705 km with an inclination angle of 98.4°, resulting in a nadir coverage from 82°S to 82°N. The satellite circles the Earth in about 98 min with an exact repeat period of 16 days. It has a nominal equator crossing time of
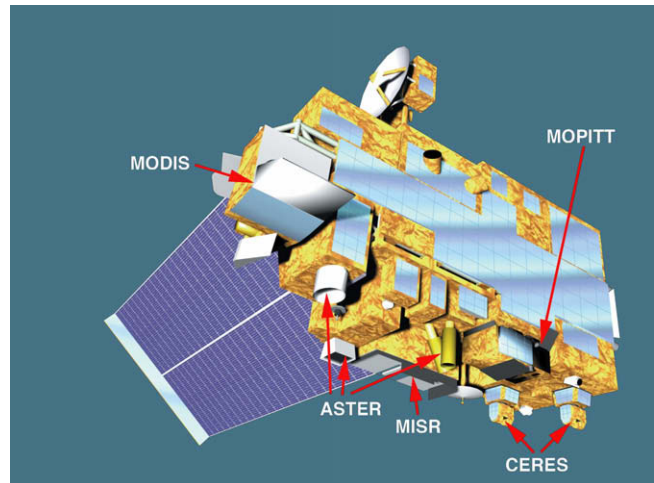

Fig. 2. The Terra spacecraft and instruments (courtesy of Marc Imhoff, NASA).

10:30 am local time in descending node. Therefore, the daytime half of the orbit is directed from northeast to southwest from the North Pole to the South Pole with the sun to the east of the satellite. The relative positions of the satellite orbit plane, the Earth center and the sun are relatively static for the sun-synchronous orbit. The satellite orbit largely dictates the instrument sampling structure in space and time.

2.2. MOPITT measurement concept

A comprehensive study of the MOPITT mission as proposed pre-launch as well as the correlation radiometer technology employed in MOPITT is given in Drummond (1996). The basic principle is the utilization of an array of correlation radiometer channels such that the thermal channels (4.7 μm) are most sensitive to upper and mid-tropospheric CO and the solar channels (2.3 μm) are most sensitive to the total CO column. These concepts will be discussed further below.

Major features of the electromagnetic energy received by the instrument are the absorptions and emissions by the atmospheric constituents at their distinctive spectral lines. A correlation radiometer such as MOPITT modulates these signals using a correlation cell such as a Length Modulated Cell (LMC) or a Pressure Modulated Cell (PMC), (both of which are described further below) containing a sample of the target gas. For each measurement a correlation gas modulator takes two samples by alternating the amount of the absorbing gas in the correlation cell between two states. Fig. 3a illustrates the two spectral samples at the two states of the correlation cell. Changes occur only in the target gas absorption lines. For the rest of the spectrum, including other contaminating gas absorption lines, the absorption is essentially unchanged. The difference of the two states as shown in Fig. 3b leaves only the changes at the correlation gas absorption lines and eliminates other
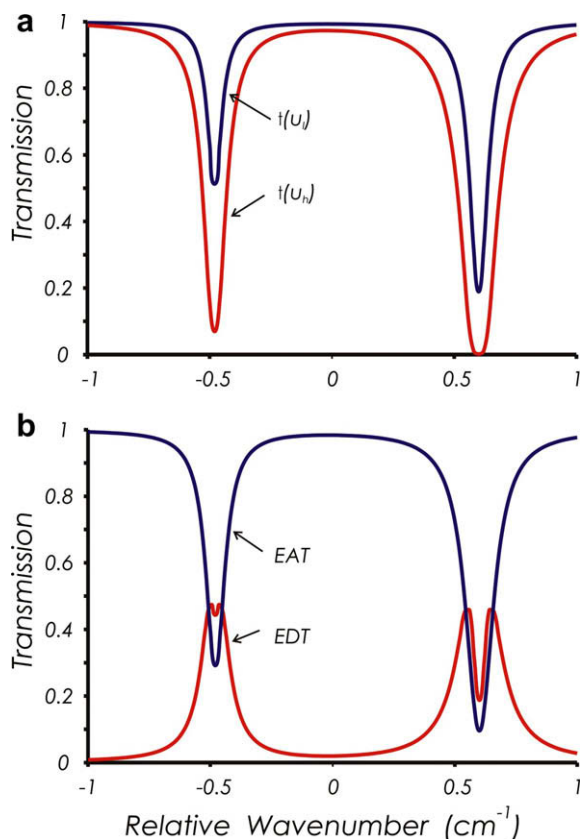
Fig. 3. (a) The spectra of two states of an idealized correlation system with a high amount of gas $\tau(u_h)$ and a low amount $\tau(u_l)$ (b) the equivalent average transmission (EAT) and equivalent difference transmission (EDT) obtained by averaging and differencing the two spectra.

components because they are not modulated between the two samples (Pan et al., 1995; Drummond, 1996; Edwards et al., 1999).

The MOPITT CO thermal channels have strong absorption characteristics (Pan et al., 1995). The difference of the two samples generated in a CO correlation radiometer measurement exhibits significant sensitivity to CO variations. The sensitivity to different layers in the atmosphere is a function of both the wavelength region and the cell pressure. However, the concentration of the gas itself in the atmosphere also modulates the sensitivity and hence the averaging kernels (Pan et al., 1998) depend upon a multiplicity of factors. A useful approximation is that a thermal channel is generally most sensitive to the target gas at a similar pressure to the gas in the correlation cell. Thus, higher pressure in the cell tends to yield more sensitivity to lower levels in the troposphere. The approach in MOPITT is to use an array of correlation cells having different pressures to derive the concentration profiles of the target gas. However, sensitivity at the lowest levels is limited not by the cell pressure but by the temperature contrast between the surface and the atmosphere which usually becomes small in the boundary layer. Some theoretical studies make the assumption that this temperature difference is zero near or at the surface (e.g. Pan et al., 1998). Under this assump-

tion the MOPITT thermal channels are sensitive to the CO mostly in the middle and upper troposphere, e.g. from 2 to 12 km. However, when the temperature contrast between the surface and the low level atmosphere is large there is significant sensitivity even in the lower troposphere. If the source of CO emission is also strong at the boundary it is still possible for MOPITT thermal channels to have useful sensitivity to the boundary layer concentrations (e.g. Deeter et al., 2007; Kar et al., 2008).

The solar channels have weak absorption characteristics (Pan et al., 1995) and do not possess the same cell pressure-related sensitivity to the atmospheric pressure distribution as thermal channels. The predominant signals are most sensitive to the total column of the target gas with a slight increase in the boundary layer (Pan et al., 1995, 1998). Overall sensitivity is increased by increasing the cell pressure within broad limits, but the averaging kernels are largely independent of cell pressure. The intention of the MOPITT project is to infer the boundary layer CO concentrations by using both the solar channels (total column) and the thermal channels (2–12 km) in a combined retrieval.

The current "Version 3" MOPITT CO profile data were derived from the thermal channels only (the solar channels are discussed further below) and are retrieved at levels of 150 mb, 250 mb, 350 mb, 500 mb, 700 mb, 850 mb and the surface for each pixel. The total column is also calculated. All these results are provided with an appropriate averaging kernel. Because the absorption occurs from the Earth's surface to the top of atmosphere, all thermal channels are correlated to some extent. To explore the number of independent pieces of information in the retrieved profiles the concept of the degrees of freedom for signals (DFS) was introduced (Rogers, 2000). The DFS obtained from the operating MOPITT thermal channels during 2000 and early 2001 is around 1.5–1.7 for daytime measurements over the tropics (Deeter et al., 2004), indicating that the MOPITT thermal channels can deliver nearly independent measurements of upper and mid-tropospheric CO, which is the essence of measuring the CO vertical structure.

2.3. Instrument description

Fig. 4 shows the MOPITT channel layout. This design achieves an optimal combination of LMCs and PMCs, thermal and solar channels, CO and CH$_4$ gases as well as allowing significant redundancy. It comprises eight channels: channels #1, #2, #3, and #4 are a group (side B) and channels #5, #6, #7 and #8 another group (side A) (note the reversal of A and B from the normal sequence). Side A and side B, although not perfect duplicates, are redundant to each other in the sense that one side can perform approximately the same function as the other side with some performance degradation. The detectors for each side are cooled by two separate coolers.

Side B (A) contains three CO channels and one CH$_4$ channel. Channel #1 (#5) and channel #2 (#6) share the
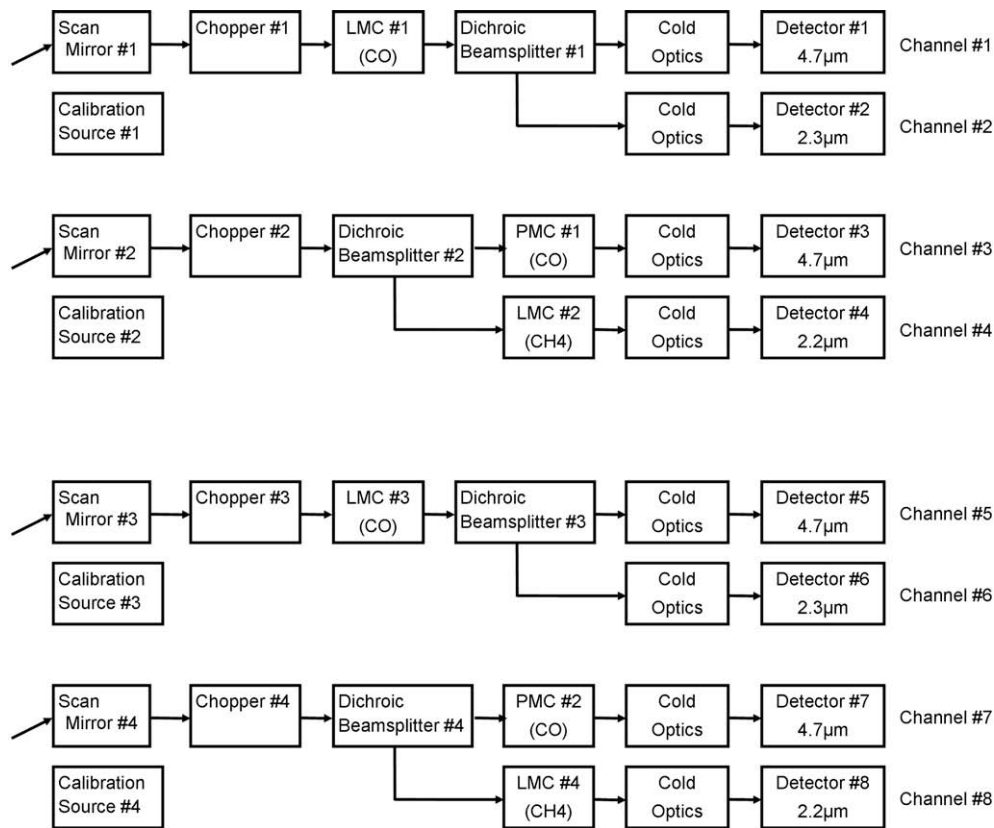
Fig. 4. Schematic diagram of the two optical tables of the MOPITT instrument. Each table holds the optical components for four channels and the detectors on each table are cooled by separate, but linked, stirling-cycle coolers.

same scan mirror #1 (#3), chopper #1 (#3) and LMC #1 (#3) with a cell pressure of 20 kPa (80 kPa). A scan mirror is the first element to receive and relay the incoming beam. It scans not only the Earth scenes but also collects observations from two calibration sources: a space view and an internal blackbody view. LMC #1 (#3) is connected a CO molecular sieve #1 (#3) that can be used to adjust the CO amount (Drummond, 1989). After the LMC the beam is split via a beam splitter #1 (#3) to reach two detectors #1 (#5) and #2 (#6). In front of each detector is a cold narrow band filter, which specifies the spectral range for the detector. Detector #1 (#5) has a central wavelength of 4.7 μm and detector #2 (#6) a central wavelength of 2.3 μm. Channel #3 (#7) and channel #4 (#8) share the same scan mirror #2 (#4) and chopper #2 (#4). Beam splitter #2 (#4) splits the beam for two modulators PMC #1 (#2) for channel #3 (#7) and LMC #2 (#4) for channel #4 (#8). PMC #1 (#2) has a working mean pressure of 7.5 kPa (3.75 kPa) and is connected with sieve #2 (#4). LMC #2 (#4) contains a CH_4 cell at a pressure of $\sim$80 kPa and no sieves. Channel #3 (#7) operates at 4.7 μm and channel #4 (#8) at 2.2 μm as determined by their respective cold filters.

The four detector arrays for each side are mounted in a detector nest in a dewar assembly and are cooled by a Stirling Cycle Cooler (SCC). Each detector array, corresponding to a channel, contains four 0.9×0.9 mm square

elements that form a linear array denoted by pixels A, B, C and D. Each pixel's square field is projected into a $1.8° \times 1.8°$ field of view (FOV) in the nadir or calibration directions. The four pixels of each detector array image four adjacent ground FOVs each with a size of approximately 22 km $\times 22$ km aligned along the direction of motion. Pixels A and D are outer pixels; pixels B and C inner pixels. All channels are co-aligned on the Earth's surface. The mirrors scan in the cross-track direction during nominal operations and produce a swath $\sim$650 km (29 pixels) wide. A near-global coverage of the Earth is provided in 3–4 days. MOPITT solar channels make valid measurements during the daytime only, while thermal channels can deliver measurements continuously.

2.4. In-flight calibration

The signals received by the detector are in form of digital counts and contain emissions from both the targets and the interfering thermal environment. An in-flight "2-point calibration" scheme (see Section 2.5.4) is realized via scanning mirrors looking at the calibration sources (space and internal blackbody). When looking at space, which has near zero radiance, the digital counts received by the detectors are generated from the emissions of the instrument and the surrounding environment. This is the offset term (S_{sp}). For any other radiance measurement,

either Earth- or blackbody-viewing, the offset term has to be subtracted first so as to derive the contributions from the sources outside of the instrument. When looking at the internal blackbody (S_{bb}), where the temperature is measured simultaneously, the radiance (R_{bb}) can be calculated using Planck's law and the known optical response function. With these two points, the gain, which is expressed as the digital count received by the detector for unit external radiance, can be derived as, in its simplest form: Gain = $(S_{bb} - S_{sp})/R_{bb}$. In this equation a precondition is that the measured voltage and radiance are linearly related. The gain is actually a comprehensive measure of the performance of the optics and detector sub-systems. The target radiance can be recovered from the measured signal S by: $R = (S - S_{sp})/$Gain.

2.5. Sub-system descriptions

2.5.1. Length modulated cells (LMCs)

The LMCs in MOPITT are the first space-borne application of this technique. The length modulator sub-system consists of the mechanical rotation system, which contains the motor, "rotor" and "compensator", the optical cell, the molecular sieve assembly and the electronic drive system (Drummond, 1996). A schematic diagram of an LMC is shown in Fig. 5. The calcium fluoride rotor in a "bowtie" shape rotates inside the cell at a constant speed of ~800 rpm and an identical compensator outside the cell rotates with a 90° phase shift to the rotor such that at any time the optical beam passes through exactly one of them. The modulation of the optical length in the cell is achieved depending on the presence or absence of the rotor in the gas cell during the passage of the beam, which corre-

sponds to the short (partial) length or long (full) length of the cell. Within one rotation there are two sets of alternating long and short length states. Each is termed a "sector". The rotor and compensator are connected via a magnetic coupling and are driven with a single motor. The stability of the modulation mechanism and a stable amount of the correlation gas over time are essential.

2.5.2. Pressure modulated cells (PMCs)

There are two PMCs operating at 3.75 kPa (PMC #2, channel #7) and 7.5 kPa (PMC #1, channel #3) used for retrieving of upper level CO in the troposphere. The pressure modulator is a fully qualified unit and has been extensively used in space applications in the past (Drummond et al, 1980). A PMC is complementary to the LMC in the sense that each has its own advantages and suitability in design and engineering realization. In general a LMC is suited for high cell gas density and a PMC for low cell gas density.

The pressure modulator sub-system consists of the mechanical compressor unit, the optical cell, the molecular sieve assembly and electronic drive system (Taylor, 1983). Fig. 6 displays the optical and mechanical layout. The pressure modulator is a mechanical device which varies the amount of gas in an optical cell by varying the pressure continually. It achieves this by the use of two linear motors (not shown in the diagram) that compress and expand the common gas volume between the two pistons, forcing it in and out of the optical cell. The length of the optical path through the cell is fixed. The "high" and "low" pressures are the two conceptual states of measurement but the pressure actually varies in a continuous cycle. The data within a cycle are pre-processed in the signal processing module (SPM) (see below) resulting in integrated high and low values. The total mass of gas in the compressor unit and the optical cell is controlled and stabilized by the use of a molecular sieve coupled with the gas cell through temperature adjustments. Sieve #2 is coupled with PMC #1 and sieve #4 coupled with PMC #2.

2.5.3. Choppers

In the MOPITT instrument a chopper is incorporated at the front-end of each of the four optical chains in order to provide a "one-point calibration". Each chopper rotates at
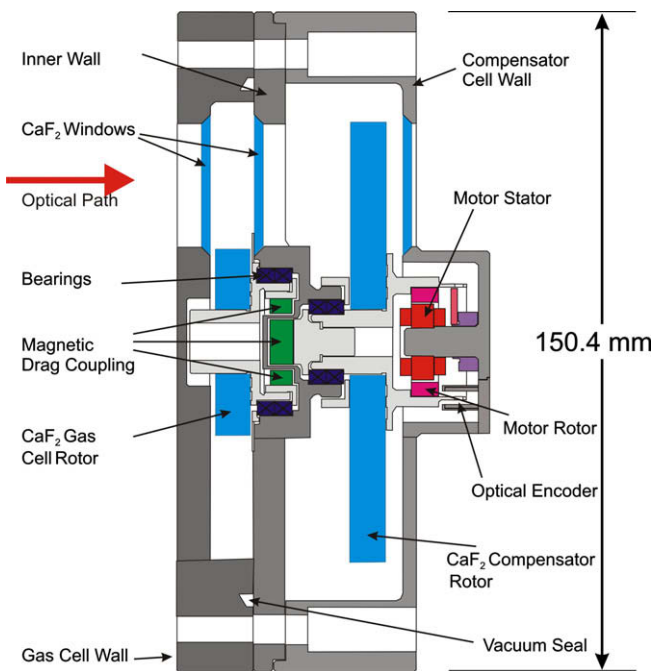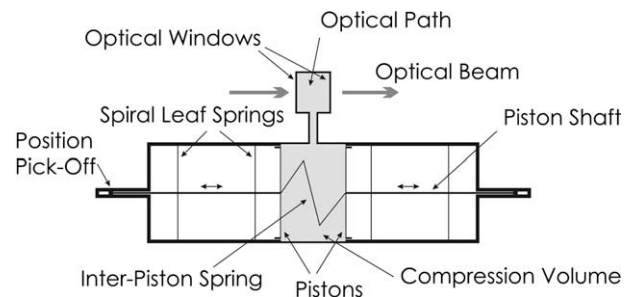

Fig. 5. Schematic diagram of an LMC.

Fig. 6. Schematic diagram of a PMC.

a constant speed of ∼1800 rpm and alternates rapidly between radiance emitted from outside the instrument ("chopper open signal" when light passes through the chopper) and from the chopper vane itself ("chopper closed signal" when light is blocked by the chopper). The times when data are recorded in the open and closed states are controlled by the blanking and processing windows (see below) and can be programmed.

2.5.4. Scanning mirrors

There are four scan mirrors mounted in front of the fore-optics. Each mirror, shared between two channels, is driven by a stepper motor and views the Earth or calibration sources in a programmed sequence. For the Earth view the mirrors scan in the cross-track direction through a range of ±25.2°, which is equivalent to a swath width of 650 km. Each view takes 0.45 s (a "stare") of which 0.4 s is for signal integration and 0.05 s for the mirror to stabilize its position. After completing 10 consecutive cycles of the Earth view, the mirrors rotate 90° to view space for five stares (2.25 s), which provides a near-zero radiance for calibrating thermal environmental changes. Immediately after each fifth space view the mirrors rotate 90° again to the opposite nadir direction to view internal blackbody targets for 20 stares (9 s), which provides a reference radiance from which the radiometric gain can be calculated.

2.5.5. Signal processing module (SPM)

There are two signal processing modules, SPM1 and SPM2, corresponding to the two sides A and B of the instrument. Each SPM digitizes, synchronously demodulates and integrates 16 optically modulated science signal inputs (4 channels and 4 pixels of each detector) from its associated optical table via the associated detector nest. The SPM is synchronized to the LMC sector, PMC state (1/2 cycle) and chopper state (open or closed). The choppers are also synchronized with their respective modulators in order to have a fixed timing relationship (Henry et al., 2001).

In order to provide the highest signal to noise, it is essential that the signals are digitized only when the optical system is stable. All channels (at launch) have high-speed choppers and the blade of the chopper takes time to move in and out of the optical path. Further, an LMC channel has interruptions in the optical signal due to the "sector transition" when the calcium fluoride rotors are entering and exiting the optical field, followed by nominally constant "valid sectors". The PMC does not have interruptions but has a signal that continually varies in the magnitude with the cell gas amount. For all these situations, the SPM defines "blanking" and "processing" windows. A blanking window is the time period of transition and is ignored and a processing window is the time of steady state and is used for signal integration. The blanking and processing windows are defined separately for the chopper open and chopper closed states and for LMC sectors. For the PMC there are two chopper states, but only one processing window each for the high and low pressure halves of the pressure cycle.

The digitizer used is a "delta–sigma" type. There are a number of reasons for this somewhat unusual choice of converter. The difference in signal for the two cell states is very small and at limiting sensitivity a resolution (averaged) of 10^{-6} is required. Hence there is a requirement for high resolution and the ability to average to higher resolution. The fast transitions of the chopper and LMC require a converter that can operate at high digitization rates and take advantage of high bandwidth electronics. It is essential that data digitized in each sector was not contaminated by "memory" of the signal from the preceding transition, i.e. it has a short settling time. A relaxed specification is that long-term DC stability is not required: long-term drift is compensated for by the calibration system. The philosophy of the signal system is to digitize the signal as soon as possible after the preamplifiers. All these requirements are met by a delta–sigma converter that has an extremely high internal linearity and a short and predictable settling time. The selected digitizer is a Motorola DSP56ADC16 converter which has 12 bits resolution in the configuration used and a settling time of ∼20 μs. More details can be found in Henry et al. (2001).

The processed signals are forwarded by the SPM to the instrument controller module (ICM) before transmission to ground as part of the low rate science (LRS) data. In a LRS data stream for a single measurement a PMC measurement contains four data entries representing high and low pressures for chopper open and closed states, while a LMC measurement contains 32 data entries representing four sectors during four rotations for chopper open and closed states.

2.5.6. Coolers

MOPITT uses two SCCs (side A and side B) mounted back-to-back to cool the eight detectors below 90 K. The SCCs were built by Astrium Limited (formerly known as British Aerospace and Matra Marconi Space). Each cooler consists of a compressor linear motor and a displacer linear motor connected with a gas tube. A cold finger mounted on the displacer is used to cool the detectors. The two coolers were mounted in-line and are driven in anti-phase to cancel the vibrations caused primarily by the compressors. Each individual compressor would have induced vibrations >40 N at a working frequency of ∼44 Hz.

2.5.7. Detectors

As discussed above, each radiometric channel of MOPITT has an array of four 0.9 mm × 0.9 mm InSb detectors that, together with the preamplifiers and optical filters are cooled to <90 K. The MOPITT detectors operate in conditions at or near those where photon statistics dominate the noise levels. The cooling of the preamplifiers assists with performance, principally through the cooling of the feedback resistor that lowers its Johnson noise, and through the consequent close proximity of the pream-

plifier to the detectors that reduces noise and microphonic effects. The cooling of the optical filter reduces the number of out-of-band photons striking the detector and therefore reduces the overall noise level.

3. On-orbit sub-system performances

3.1. Overall stability

The MOPITT instrument design is inherently very temperature stable. The major heat rejection is through the base-plate to an ammonia capillary-pumped refrigerator system, which rejects the heat to a radiator mounted below the instrument. These services were provided by the Terra spacecraft and are to a certain extent legacies from the Polar Orbiting Platform concept from the early days of the Earth Observing System program. When the satellite design was changed, this heat regulation system was retained for both MOPITT and ASTER.

The effect of this system is to give MOPITT remarkable thermal stability. A typical 3-day plot of the base-plate temperature is shown in Fig. 7. There is a predominantly sinusoidal component with a peak to peak amplitude of 0.7 K at the orbital period of 98 min. The maximum rate of change is ~0.23 mK/s. The peak occurs at the South Pole and the trough at the North Pole; when the satellite flies from the North Pole to the South Pole on a descending pass the instrument is constantly illuminated by the sunlight and thus heats up. Instrument temperature reaches a maximum over the South Pole. On the ascending pass the opposite situation occurs. The temperature also oscillates with an amplitude ~0.1 K at a period of about 24 h. This is the effect of the Earth's thermal emission on the instrument. After approximately 24 h, the satellite returns to a path close to its original orbit and the Earth "illuminates" the satellite upwards out of a similar thermal environment. The low rate of change of temperature and its smooth var-

iation pattern translate into a stable and predictable instrument condition through time and reliable calibrations as outlined below can be performed in the data processing procedure.

3.2. Length modulator sub-systems

The operation of the LMC sub-systems is fully autonomous. The major parameters to monitor are the motor current, and the cell pressure and temperature which together determine the density of the gas in the cell. The motor current (not shown) has been essentially constant throughout the mission. The original requirement for the instrument is 5 years of life time, i.e. 2×10^9 rotations for the motor. The actual performance has exceeded the requirement with 3.8×10^9 rotations so far. The temperature and the pressure of LMC #3 are shown in Fig. 8a and b, respectively. The temperatures of the LMCs are all within a range of 295–300 K. The daily averaged temperature shows a slowly decreasing long term trend, but has less than a one degree variation over the mission. It is uncertain whether this slow
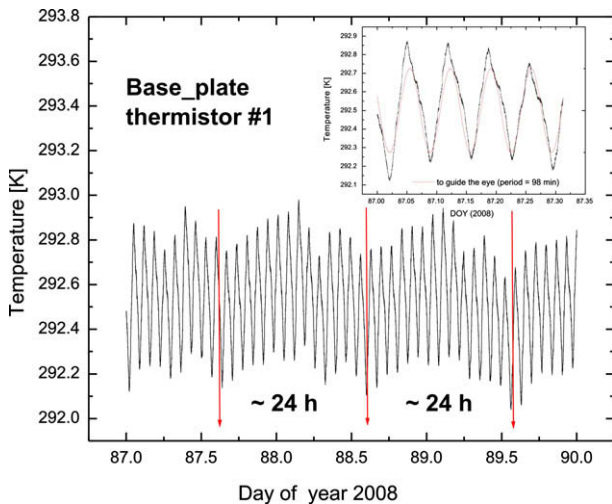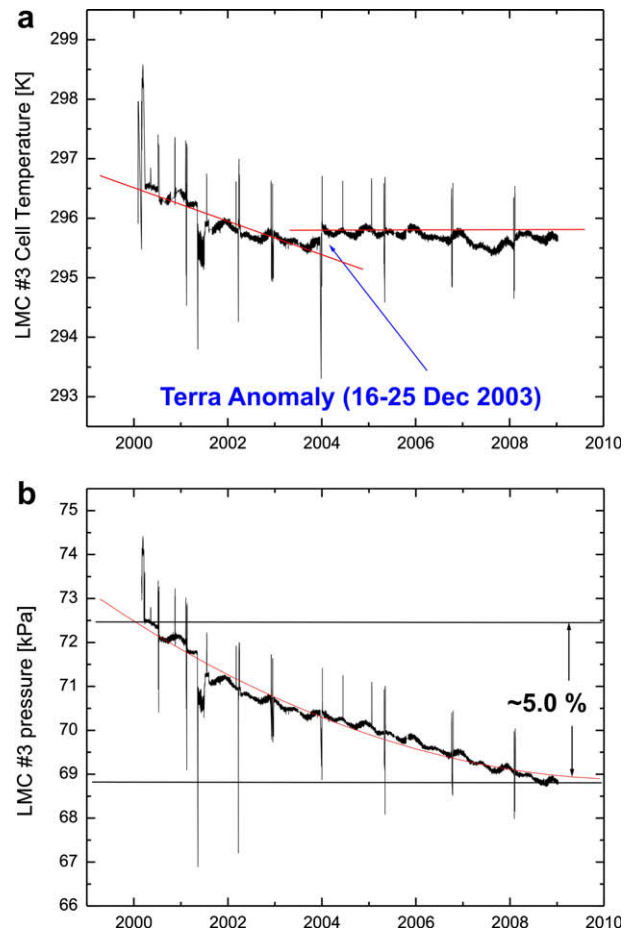
Fig. 8. LMC #3 temperature (K) (a) and pressure (kPa) (b) time series over the entire mission from 2000 to 2008. Each data point represents an average over one day. The spikes correspond to the decontamination and hot calibration operations.

Fig. 7. Typical 3-day time series of the base-plate temperature.

decreasing trend is a real temperature variation or an artifact of sensor or circuit drift. What is certain is that the long term trend is fairly small, well within the health range for operating. There was an abrupt temperature drop in May 2001 when one cooler failed to operate and the entire instrument was shut down for two months and operation resumed in a different configuration (more details in Section 3.6). There was another temperature shift of 0.2 K at the end of 2003 when a Terra anomaly unrelated to MOPITT occurred. The pressure of LMC #3 also has a slightly decreasing trend at the rate of ~0.4 kPa per year and has dropped ~5% in 9 years. This loss of the gas is within the tolerance range and no adjustments of the cell pressure have been made using the associated molecular sieve.

The performances of LMC #1, #4 are similar to LMC #3 and their trend plots of motor current, temperature and pressure are not shown here. Starting from the middle of 2001 the gas pressure in LMC #2 gradually decreased and dropped near zero by the end of 2005. The decrease starts around May 2001, coincident with the cooler failure, but no conclusions can be drawn from this coincidence.

3.3. Pressure modulator sub-systems

Both the PMC #1 and #2 have operated without anomaly during the mission. The PMC amplitudes (not shown here) are stable over the mission. There are two phases: in the first phase before cooler failure (see Section 3.6) it was set at 4.6 mm and then in the second phase it was changed to the maximum stroke of 6.35 mm to enhance the signal of PMC #2. Fig. 9 shows the PMC #2 motor current for the nine years of operation. In the second phase there is a 9% decrease of the motor current over six years which could be due to a number of causes such as a slight resonance shift within the PMC or an increase in position sensor gain (Caldwell et al., 2005). The pressure is an important parameter but because there was no available high reliability gauge for the low pressure of the PMC there is no telemetry directly monitoring the pressure in the cell. The mean pressure of the gas and its trend are crucial parameters for the retrieval: they are determined by performing the "PMC sweeps".

The purpose of the PMC sweeps is to derive the "resonant frequency" of the PMC. The mean pressure is related to the resonant frequency via an empirical formula obtained during pre-launch calibration activities. In a PMC sweep a pre-defined set of frequencies is scanned using different amplitudes. From these the frequency versus motor current relationship is established. The minimum current corresponds to the resonant frequency. In practice two sieve temperatures are used, one lower than the current operating sieve temperature and the other higher, bracketing the nominal operating point. From multiple scans a multiple-variant array is established among the scan parameters including resonant frequency, minimum motor current, sieve temperature, and PMC amplitude. A regression formula derived from the pre-launch data is used to determine the operating pressure. Over the mission period eight PMC calibrations have been performed and the derived mean pressures for PMC #2 are shown in Fig. 10. The first three occurred before May 2001 and the other five in the second phase when PMC #2 amplitude was increase to its maximum stroke. There is a continuous decrease of the mean pressure in the second phase for ~6% over six years, indicating a possible gas leakage in PMC #2. The PMC #2 mean pressure change seems consistent with the PMC #2 motor current decrease (Fig. 9) under the condition of constant stroke, but this relationship has not been fully investigated.

The high and low pressures in the gas cell, although not monitored simultaneously, can be inferred from the stroke amplitude along with the mean pressure.
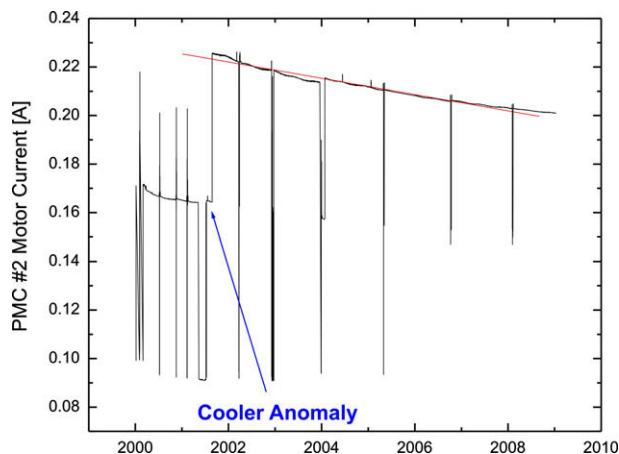

Fig. 9. PMC #2 motor current over the mission from 2000 to 2008 consists of two phases: the first before the cooler anomaly on May 7, 2001 and the second after the recovery from the cooler anomaly.
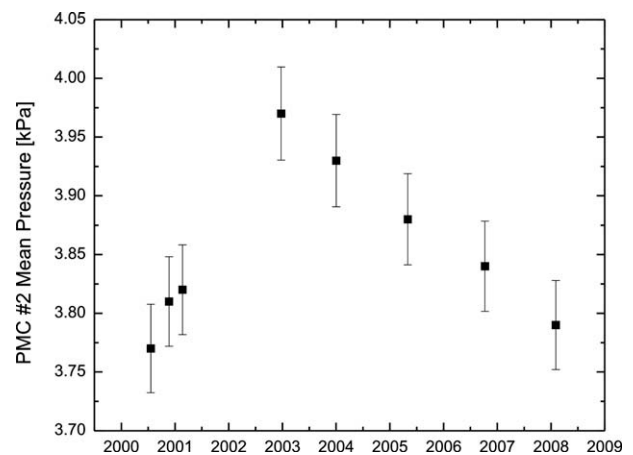

Fig. 10. PMC #2 working pressures derived when PMC frequency sweeps were performed. The vertical bars represent the standard deviations.

3.4. Choppers

When the instrument is in orbit the chopper closed signals show very small variations compared to chopper open signals; a further confirmation that the instrument is in an extremely stable thermal environment. Moreover, the offset term obtained from the space view, although sampled once per 130 s, provides an effective calibration for accounting for the thermal drift effect to the first order. These two factors essentially could eliminate the requirement for the chopper closed signals. On August 4, 2001 chopper #3, which was shared by channels #5 and #6 failed to operate. Fortunately, it stopped at a completely open position allowing us to verify the discussion above and to demonstrate that reconfiguration of the data processing without the chopper results in lower noise equivalent radiance. Stopping the remaining choppers is not a possibility because there is no defined mechanism to ensure that a chopper stops in a completely open position.

3.5. Scanning mirrors

The two functions for each scanning mirror for both Earth sampling and calibration have been proven effective and efficient. Mirrors #2, #3, #4 have been operating nominally. Mirror #1, however, stopped working on April 6, 2002 after two years of operation. The cause of the failure could not be identified.

3.6. Cooler performance

After launch the coolers initially performed nominally. However, on May 7, 2001 the displacer on side B hit the end stop causing the cooler system to autonomously shut down. A series of diagnostic tests revealed that the side B displacer did not respond to any drive commanding and was actually being driven by the pressure wave generated in compressor B. It has not been possible to pinpoint the exact cause of the failure. Possible candidates include an open circuit in the displacer electronics, wiring harness or mechanism. As a result channels #1–#4 could not deliver useful measurements because they could not be cooled. It was not possible to operate side A cooler alone because of the high level of vibration that would be induced in the spacecraft. The side B compressor must be operated as well in order to compensate for the vibration of compressor A, and it must also be operated at a low enough amplitude to avoid the displacer B hitting the end stop. The final operating mode used was a slightly unbalanced mode where compressor B operates at 82.5% of the nominal stroke (~6.5 mm), which allows displacer B to oscillate but not to strike the end stop, and compressor A as shown in Fig. 11 (red curves) operates at a slightly reduced amplitude of 6.2–6.35 mm after the recovery from the cooler failure compared to the nominal 6.4–6.9 mm. Displacer A amplitude was also enhanced from the nominal 2.68 mm to 3 mm in order to have more cooling capacity. Channels
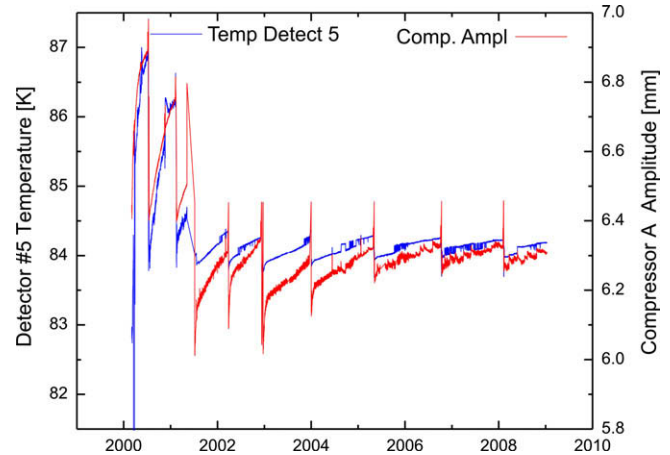

Fig. 11. Detector #5 temperature (blue and generally upper) and the compressor A amplitude (red and generally lower) time series over the entire mission from 2000 to 2008. Each increasing segment in the temperature and amplitude plots begins and ends with a decontamination and hot calibration event.

#5–#8 have been operating successfully for a total of more than 7 years in this manner.

3.7. Detectors

Fig. 11 (blue curves) shows the temperature history of detector #5 over the entire mission. The temperature evolution is a sequence of segments of increasing temperature. The increase of temperature over time is caused by gradual ice buildup on the cold optics in the detector nest increasing the thermal leak to the structure. The temperature increase is also consistent with an observed increase in compressor A amplitude (Fig. 11, red curves). Between the temperature segments is a decontamination event when the cooler is turned off for ~48 h, which allows the detector to warm room temperature ~300 K and thus removes the ice. Fig. 11 shows that as the mission has progressed the rate of temperature increase has slowed indicating that the instrument environment is getting cleaner/drier over time. The decontamination operation is thus required less frequently, reducing from the initial requirement of once every 3–4 months to the current annual requirement. This time interval is also driven by the need for PMC sweeps and for the operators to remain familiar with the procedure.

4. In-flight channel performances

4.1. Overall performance of the thermal channels

The MOPITT thermal (4.7 μm) channels are very sensitive to the in-flight thermal environment. The 2-point calibration scheme discussed earlier is specifically designed for thermal channel calibrations. The space view signal is sampled every 130 s and the blackbody view every 11 min

immediately after a space view. The sampling rate of the blackbody view is therefore the rate for updating the gain calculation. The blackbody is maintained at near room temperature, which is suitable for all thermal channel gain calculations.

Fig. 12a shows a typical 2-day time series of the offset term S_{sp} of the averaged signal of the two states of the PMC for channel 7 pixel A. The curve clearly shows a sinusoidal component at the orbital period. This orbital variation is consistent with the temperature changes of the instrument as outlined above. The offset also oscillates at a longer time scale of $\sim$24 h, again consistent with the instrument temperature changes at the same time scale.

The corresponding gain plot is shown in Fig. 12b. Ideally, the orbital and 24-h variations should not be present in the plot. The gain is a function of the instrument characteristics and is not related to external environmental factors. However, there is a small twice per orbit component

in the gain of peak-to-peak magnitude $\sim$0.1%. The most probable cause of this oscillation is that the blackbody is not perfect: upward Earth emission can enter the blackbody and be reflected back into the detector.

Channel 7 is the only thermal channel that is unaffected by both the cooler fault and the chopper #3 issue, and we can therefore study the gain under uniform conditions for the entire mission. Fig. 13a shows the long-term gain trend of the total signal for channel #7 pixel A over the entire mission period. In the plot we took a 2-h average sample for each day, neglecting fluctuations on time scales shorter than one day such as the twice per orbit variations. The gain trend is a sequence of decreasing segments and is anti-correlated with the detector temperature trend shown in Fig. 11 because both are attributed to the same reason: the ice buildup on the cold optics that reduces the optical transmission. The de-contamination that removes the ice also recovers the gain. The plot shows that the gain of this channel in
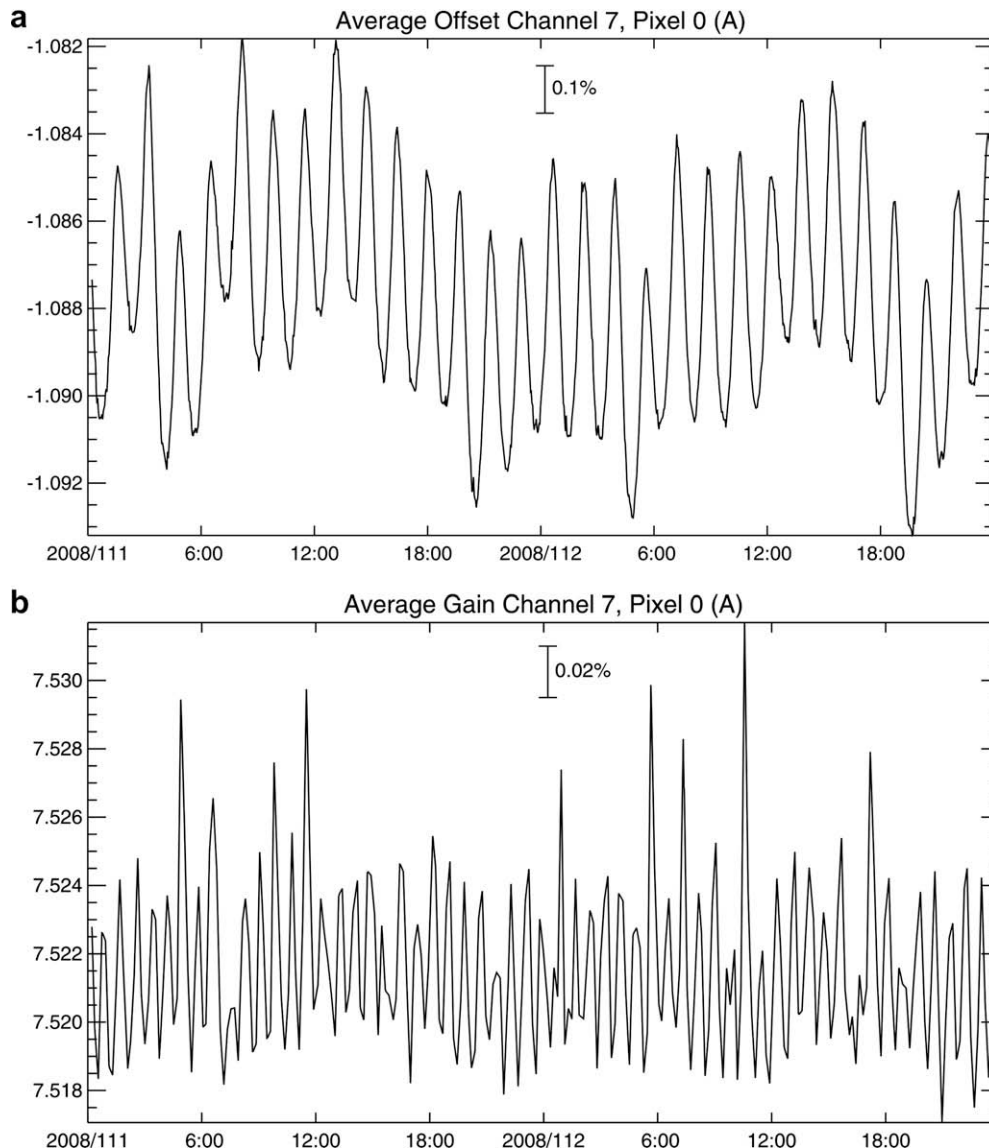

Fig. 12. Typical 2-day plots of (a) the offset and (b) the gain of the average signal of channel 7 pixel A.
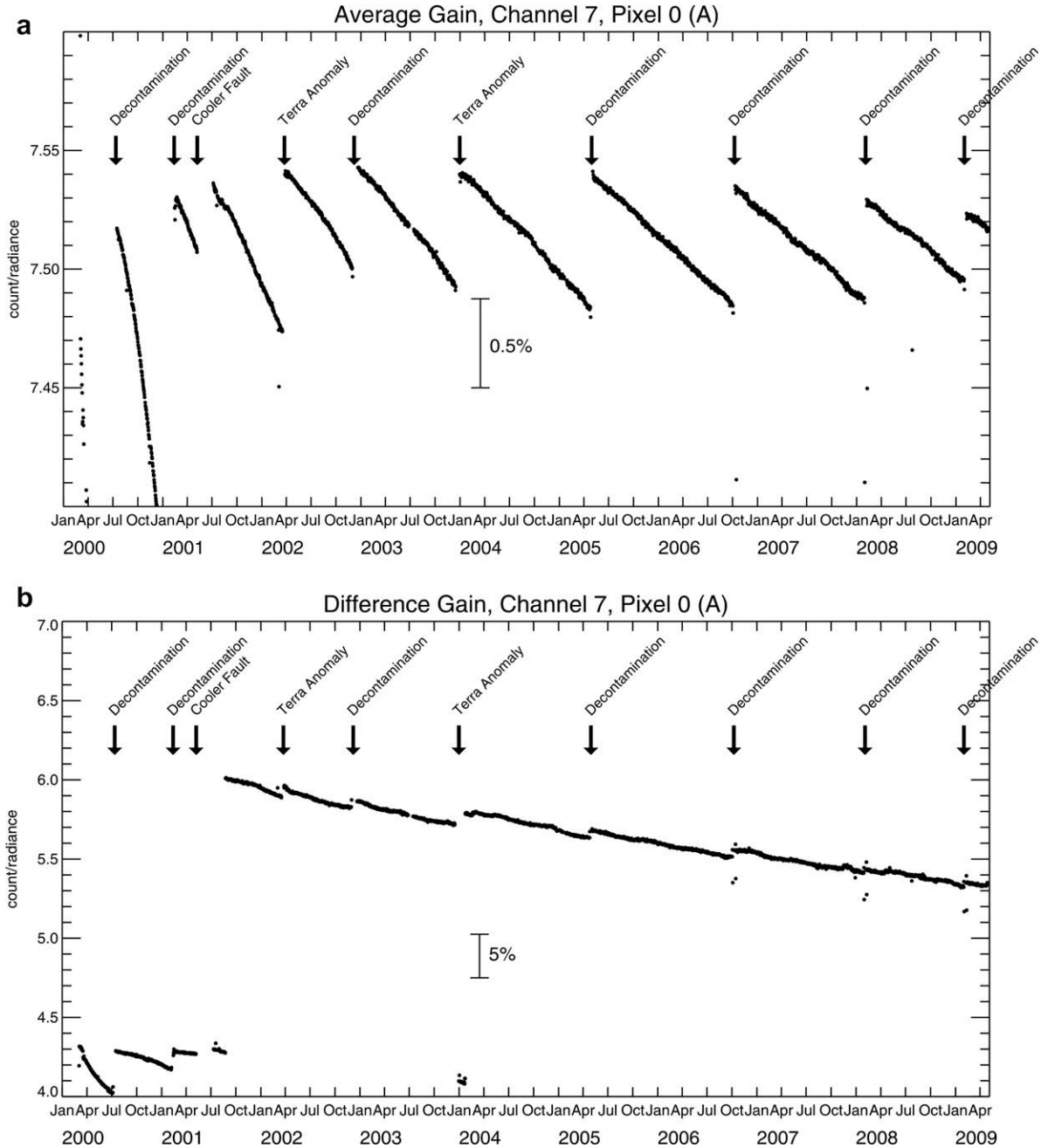
Fig. 13. Long-term trends of (a) the average and (b) the difference gains for channel 7 pixel A. Each decreasing segment begins and ends with a decontamination and hot calibration operation. The jump in the difference gain in late 2001 is a consequence of the change in PMC amplitude after the cooler anomaly.

the uncontaminated state (the top envelope portion) has decreased by less than 0.2% over the 9 year mission.

Fig. 13b is the long-term gain trend of the difference signal for channel #7 pixel A. The decreasing trend of each segment between two decontamination events is similar to that in the total signal gain trend for the same reason (Fig. 13a). However, the maxima show a steady decrease ∼15% over the 7.5 years since late 2001, indicating there is a drift in channel 7 with a cause other than contamination. Gas leakage in PMC #2 (Fig. 9b) will lead to difference gain drop, but gas leakage alone cannot fully

explain the difference gain decrease and other optical and/or electronic effects must be occurring. The jump in the difference gain in late 2001 is a consequence of the change in PMC amplitude after the cooler anomaly (see Section 3.3).

The composition measurements deduced from MOPITT measurements are very sensitive to changes in the instrument, so even if the instrument performs well from an engineering standpoint, the scientific data may show variations. A recent MOPITT validation study (Emmons et al., 2009) showed that there is ∼20% positive bias of MOPITT

retrieved CO (Version 3 data) comparing to in situ aircraft measurements accumulated over a period from the mission start to 2006. Multiple factors can contribute to this bias in the retrieval, including the pressure decreases in both LMC #3 and PMC #2. Since the instrument life was expected to be only five years, time-varying instrument parameters were not incorporated in the Version 3 data processing and this could be part of the source of the bias. Version 4 processing (probably current when this paper is published) will account for this variation. Future validation work is expected to re-assess the long term trending of MOPITT retrieved CO.

4.2. Overall performance of the solar channels

The solar channels (2.2 μm and 2.3 μm) are much less sensitive to the thermal environment than the thermal channels. Valid solar channel measurements occur only during daytime. The offset term during the daytime obtained from the space view is much less than the signal from the Earth scenes. A constant offset by averaging the daytime offset samples is appropriate. Similar to the thermal channels the solar channel gains are also the function of characteristics of associated optics and detector sub-systems, having no correlations to external factors. The major factor affecting the solar channel gain is the contamination on the cold optics in the detector nest, i.e. the ice buildup over time. The contamination is a slow process, therefore, less frequent calibration is required. To obtain the solar channel gain, the blackbody has to be heated up to 460 K in order to get sufficient signal. This is called the "hot calibration". MOPITT hot calibrations are carried out just before and after each decontamination. As for the thermal channels the gain obtained after the decontamination is enhanced to its maximum, while the gain before the next decontamination is at its minimum value. The gain between these two points is calculated by linear interpolation.

Over the mission time most of the scheduled hot calibrations were performed successfully. However, there are several missing points. For example, the July 13, 2000 hot calibration, which was performed after a successful decontamination, did not produce valid data because of an error in setting up the MOPITT computer. Other examples are the cooler failure on May 7, 2001 and a Terra anomaly of out-of-limits yaw rate on December 16, 2003. Both the instrument and spacecraft anomalies have the same effect of a decontamination operation as the instrument was unexpectedly forced to shut down causing all of the detectors to warm up passively. The pattern and trends in the solar channel gains (not shown here) are consistent with the thermal channels.

4.3. Correction of the filter profiles

There is a cold narrow band pass filter in front of each detector to isolate the optical band of interest. The MOPITT filters are multi-layer interference filters and are the only narrow band pass filters in the optical chain. The transmission was provided by the manufacturer at temperatures of 300 K and 105 K (McKernan, 2002). The manufacturer also provided theoretical temperature shift coefficients and expected shifts for a range of input angles of the filters.

An early retrieval study (Deeter et al, 2001) using the manufacturer filter profiles resulted in biased CO distribution and unrealistic pairing pattern between the inner and outer pixels. McKernan (2002) carried out an extensive study of the filters' conditions in the in-flight environment. As a result of this study two corrections were applied: (1) an appropriate temperature correction for detector/filter temperatures on orbit: 92 K for channels #1–#4 and 87 K for channels #5–#8; (2) a correction for changes in the filter pass band due to the fact that mean angle of incidence for the inner and outer pixels on the filter are 2° and 5.6° off normal, respectively. After these corrections were applied, the bias and pairing features in the CO retrieval were resolved.

Since the filters are thermally sensitive, the drift in temperature due to water vapor contamination of the cold system (see above) is a potential issue for the instrument. This was resolved by establishing one criterion for performing decontamination procedure as being when the detector systems rose in temperature by 1 K. Temperature in the detector system now rises so slowly that this criterion is no longer relevant and the overall time criterion (<1 year) determines the detector decontamination interval.

4.4. Solar channel challenges

So far MOPITT has not released any CO or methane column data. The total column of CO in Version 3 data is weighted by an averaging kernel that is less sensitive to CO in the lower levels. It was not until recently that CO solar channel #6 was demonstrated capable of retrieving CO total column (Deeter et al., 2009). Over the oceans sun glint and polarization effects caused by the specular reflection of the sunlight from the surface cause small unpredictable shifts in the signal. The low reflectivity of ocean surface and some types of land results in low signal to noise ratio. In a LMC the radiances in the two states are obtained from two measurements at slightly different times as the rotor rotates. The two FOVs on the Earth shift by ∼175 m given that the rotor with four sectors rotates four times for a stare of 0.4 s and the satellite moves at a ground speed of 7 km/s. Inhomogeneity of the underlying surface reflectance of the two scenes contributes to excessive noise level (dubbed "geophysical noise"). This is particularly significant over land. There are also other factors such as spectral dependence of the reflectance (Pfister et al., 2005) that may contribute additional noise.

Despite these problems MOPITT CO solar channel data has demonstrated to be capable of retrieving the CO total column by applying an optimal estimation algorithm that solves for CO profiles that are statistically consistent with

the observation and an a priori profile (Deeter et al., 2009). The effective measurement noise is higher than predicted from pre-launch calibrations and so empirically determined noise values are used. Case studies over land areas show that solar channel retrieved CO total columns not only capture major features of the operational thermal channel CO, but contain finer structures that are left for further validation.

5. Perspectives for future instrumentation

Nine years of operation of the MOPITT instrument clearly delineates the strengths and the weaknesses of the design approach. Failures always involved moving parts such as the stepper motor of scanning mirror #1, the motor of chopper #3 and the displacer of cooler B. As shown in Section 3.4, choppers are unnecessary parts if thermal stability is adequate. In a future design the thermal stability should be sufficient to avoid the need for choppers. An alternative to the scanning mirror is the utilization of larger array detectors, which have a larger footprint on the ground and require reduced scanning ranges or no scanning at all. Over the past decade newer technologies have been demonstrated including the passive cooling used on the ACE instrument in SciSat-1 rather than the active coolers employed in MOPITT. This kind of technology should be investigated further, but the orientation of the radiative cooler may be problematic. The detectors on MOPITT had four elements, InSb detectors cooled to 90 K. They are working well and have a quantum efficiency of >0.9. Unless alternate detectors offer other advantages, such as a higher working temperature, these should be retained. The preamplifiers in MOPITT were also cooled and this led to lower microphonic effects (shorter wiring with low-level signals) and higher performance.

The MOPITT concept of using an array of correlation gas radiometers to retrieve CO profiles is a success and could be applied with advantage for the future mission. Both the high pressure LMC and the low pressure PMC were demonstrated to be reliable and successful over the mission. Relatively speaking, a PMC is more difficult to operate on-orbit than a LMC due to requirement of PMC sweeps to determine the mean pressure in the cell. A pressure sensor for the mean pressure or preferably the entire pressure cycle would be advantageous. A low pressure LMC could be considered to replace the high pressure PMC under some engineering constraints. Further studies on the issue of how many channels are optimal in achieving a balance between more degrees of freedom for signals (DFS) in the CO profile and avoiding inefficient channels should be made: a low and a high pressure thermal channel together capture most of the upper and mid layer tropospheric CO. The MOPITT solar channels suffer from excessive geophysical noise and polarization effects over ocean that are the main obstacles in delivering high quality CO total column data. To retrieve CO at the lowest levels in the atmosphere, solar channels must be incorporated and the engineering challenges must be overcome. In a future design some modifications should be considered, particularly for solar channels. For example, it would be very advantageous to enable simultaneous measurements of the two states in order to effectively remove the geophysical noise.

The coverage in space and time, field-of-view and vertical resolution are intertwined via the size of the optical system and the signal-to-noise ratio desired. The solution used for MOPITT has enabled a considerable amount of science to be performed. Future missions could focus on higher time resolution – for example by going to geostationary orbit – or higher spatial resolution which would still be best performed from the low Earth orbit. There is no "perfect mission" that can obtain global coverage, high temporal resolution, high spatial resolution and vertical sensitivity and therefore a combination of missions will be required.

Redundancy has proved to be valuable to the MOPITT mission, enabling it to continue in the presence of significant mechanism failures. The redundancy philosophy is somewhat dependent upon the mission proposed lifetime and "probability of success" requirements imposed at the top level of mission management, however, the redundancy in MOPITT has proved useful for the longevity of the mission.

6. Conclusions

The MOPITT instrument has demonstrated the ability to measure CO over the planet on a continuous basis for an extended period of time. Science processing of the data has enabled advances in our understanding of the production and transport of pollutants on regional and global scales.

From an engineering point of view, the mechanisms in MOPITT have provided the required support to the mission. Experience gained from this extended continuous period of operation can be applied to future generations of similar instruments.

Acknowledgements

References

Beer, R., Glavich, T.A., Rider, D.M. Tropospheric emission spectrometer for the Earth Observing System's Aura Satellite. Appl. Optics 40 (15), 2356–2367, 2001.

Bernath, P., McElroy, C.T., Abrams, M.C., Boone, C.D., Butler, M., et al. Atmospheric chemistry experiment (ACE): mission overview. Geophys. Res. Lett. 32, L15S01, doi:10.1029/2005GL022386, 2005.

Buchwitz, M., Schneising, O., Reuter, M., Bovensmann, H., Burrows, J.P. Global carbon monoxide as retrieved from SCIAMACHY by WFM-DOAS. Atmos. Chem. Phys. 4, 1945–1960, 2004.

Caldwell, D., Hackett, J., Gibson, A.S., Drummond, J.R., Nichitiu, F. The design and flight performance of the MOPITT instrument mechanisms, in: Proceedings of 11th ESMATS, 2005.

Chahine, M.T., Pagano, T.S., Aumann, H.H., et al. AIRS: improving weather forecasting and providing new data on greenhouse gases. Bull. Am. Meteorol. Soc. 87 (7), 911–926, 2006.

Clerbaux, C., Edwards, D.P., Deeter, M.N., Emmons, L., Lamarque, J.-F., Tie, X.X., Massie, S.T., Gille, J. Carbon monoxide pollution from cities and urban areas observed by the Terra/MOPITT mission. Geophys. Res. Lett. 35, L0817, doi:10.1029/2007GL032300, 2008.

Deeter, M.N., Emmons, L.K., Edwards, D.P., Gille, J.C., Drummond, J.R. Vertical resolution and information content of CO profiles retrieved by MOPITT. Geophys. Res. Lett. 31, L15112, doi:10.1029/2004GL020235, 2004.

Deeter, M.N., Edwards, D.P., Gille, J.C., Drummond, J.R. Sensitivity of MOPITT observations to carbon monoxide in the lower troposphere. J. Geophys. Res. 112, D24306, doi:10.1029/2007JD008929, 2007.

Deeter, M.N., Edwards, D.P., Gille, J.C., Drummond, J.R. CO retrievals based on MOPITT near-infrared observations. J. Geophy. Res. 114, doi:10.1029/2008JD010872, 2009.

Drummond, J.R. Novel correlation radiometer: the length modulated radiometer. Appl. Opt. 28, 2451, 1989.

Drummond, J.R. MOPITT Mission Description Document. The University of Toronto, Toronto, Ontario, 1996.

Drummond, J.R., Houghton, J.T., Peskett, D.G., Rodgers, C.D., Wale, M.J., Whitney, J., Williamson, E.J. The stratospheric and mesospheric sounder on NIMBUS 7. Philos. Trans. Roy. Soc. Lond. Ser. A 296, 219–241, 1980.

Edwards, D.P., Halvorson, C.M., Gille, J.C. Radiative transfer modeling for the EOS Terra Satellite Measurement of Pollution in the Troposphere (MOPITT) instrument. J. Geophys. Res. 104, 16755–16775, 1999.

Edwards, D.P., Emmons, L.K., Hauglustaine, D.A., Chu, D.A., Gille, J.C., Kaufman, Y.J., Pétron, G., Yurganov, L.N., Giglio, L., Deeter, M.N., Yudin, V., Ziskin, D.C., Warner, J., Lamarque, J.-F., Francis, G.L., Ho, S.P., Mao, D., Chen, J., Grechko, E.I., Drummond, J.R. Observations of carbon monoxide and aerosols from the Terra satellite: Northern Hemisphere variability. J. Geophys. Res., 109, D24202, doi:10.1029/2004JD004727, 2004.

Edwards, D.P., Emmons, L.K., Gille, J.C., Chu, A., Attié, J.-L., Giglio, L., Wood, S.W., Haywood, J., Deeter, M.N., Massie, S.T., Ziskin, D.C., Drummond, J.R. Satellite-observed pollution from Southern Hemisphere biomass burning. J. Geophys. Res. 111 (D16303), doi:10.1029/2006JD007079, 2006a.

Edwards, D.P., Pétron, G., Novelli, P.C., Emmons, L.K., Gille, J.C., Drummond, J.R. Southern Hemisphere carbon monoxide interannual variability observed by Terra/Measurements of Pollution in the Troposphere (MOPITT). J. Geophys. Res. 111 (D16303), doi:10.1029/2006JD007079, 2006b.

Emmons, L.K., Edwards, D.P., Deeter, M.N., Gille, J.C., Campos, T., Nédélec, P., Novelli, P., Sachse, G. Measurements of Pollution in the Troposphere (MOPITT) validation through 2006. Atmos. Chem. Phys. 9, 1795–1803, 2009.

Froidevaux, L., Livesey, N.J., Read, W.G., et al. Early validation analyses of atmospheric profiles from EOS MLS on the Aura satellite. IEEE Trans. Geosci. Remote Sens. 44 (5), 1106–1121, 2006.

Gunson, M.R., Abbas, M., Abrams, M.C., Allen, M., Brown, J.R., Brown, T.L., et al. The Atmospheric Trace Molecule Spectroscopy (ATMOS) experiment: deployment on the ATLAS Space Shuttle missions. Geophys. Res. Lett. 23, 2333–2336, doi:10.1029/96GL01569, 1996.

Henry, D., Hackett, J., Drummond, James R., Colley, R. Timing control and signal processing design of the MOPITT instrument, in: Proceedings of SPIE, Infrared Spaceborne Remote Sensing IX, 1–3 August 2001, San Diego, USA, pp. 131–139, 2001.

Kar, J., Bremer, H., Drummond, J.R., Rochon, Y.J., Jones, D.B.A., Nichitiu, F., Zou, J., Gille, J.C., Edwards, D.P., Deeter, M.N., Francis, G., Ziskin, D., Warner, J. Evidence of vertical transport of carbon monoxide from Measurements of Pollution in the Troposphere (MOPITT). Geophys. Res. Lett. 31, L23105, doi:10.1029/2004GL021128, 2004.

Kar, J., Drummond, J.R., Jones, D.B.A., Liu, J., Nichitiu, F., Zou, J., Gille, J.C., Edwards, D.P., Deeter, M.N. Carbon monoxide (CO) maximum over the Zagra Mountains in the Middle East: signature of mountain venting? Geophys. Res. Lett. 33, L15819, doi:10.1029/2006GL026231, 2006.

Kar, J., Jones, D.B.A., Drummond, J.R., Attié, J.L., Liu, J., Zou, J., Nichitiu, F., Seymour, M.D., Edwards, D.P., Deeter, M.N., Gille, J.C., Richter, A. Measurement of low altitude CO over the Indian subcontinent by MOPITT. J. Geophys. Res., 113, D16307, doi:10.1029/2007JD009362, 2008.

Kobayashi, H., Shimota, A., Kondo, K., Okumura, E., Kameda, Y., Shimoda, H., Ogawa, T. Development and evaluation of the interferometric monitor for greenhouse gases: a high throughout Fourier-transform infrared radiometer for nadir Earth observation. Appl. Opt. 38, 6801–6807, 1999.

Liu, J., Drummond, J.R., Jones, D.B.A., Cao, Z., Bremer, H., Kar, J., Zou, J., Nichitiu, F., Gille, J.C. Large horizontal gradients in the atmospheric CO at the synoptic scale as seen by space-borne measurements of pollution in the troposphere. J. Geophys. Res. 111, D02306, doi:10.1029/2005JD006076, 2006.

McKernan, E. MOPITT spectral characterization and forward modeling, Ph.D. Thesis, Department of Physics, University of Toronto, 2002.

Pan, L., Edwards, D.P., Gille, J.C., Smith, M.W., Drummond, J.R. Satellite remote sensing of tropospheric CO and CH₄: forward model studies of the MOPITT instrument. Appl. Optics 34 (30), 6976–6988, 1995.

Pan, L., Gille, J.C., Edwards, D.P., Bailey, P.L., Rodgers, C.D. Retrieval of carbon monoxide for the MOPITT instrument. J. Geophys. Res. 103 (32), 277–332, 290, 1998.

Pfister, G., Gille, J.C., Ziskin, D., Francis, G., Edwards, D.P., Deeter, M.N., Abbott, E. Effects of a spectral surface reflectance on measurement of backscattered solar radiation: application to the MOPITT methane retrieval. J. Atmos. Ocean Technol. 22, 566–574, 2005.

Reichle, H.G., Anderson, B.E., Connors, V.S., Denkins, T.C., Forbes, D.A., Gormsen, B.B., Langenfelds, R.L., Neil, D.O., Nolf, S.R., Novelli, P.C., Pougatchev, N.S., Roell, M.M., Steele, L.P. Space shuttle based global CO measurements during April and October 1994, MAPS instrument, data reduction and data validation. J. Geophys. Res. 104 (D17), 21,443–21454, 1999.

Rogers, C.D. Inverse Methods for Atmospheric Sounding, Theory and Practice. World Scientific, Singapore, 2000.

Taylor, F.W.. Pressure Modulator Radiometry, Spectrometric Techniques, vol. III. Academic Press, New York, pp. 137–197, 1983.

Turquety, S., Hadji-Lazaro, J., Clerbaux, C., Hauglustaine, D.A., Clough, S.A., Cassé, V., Schlüssel, P., Mégie, G. Operational tracer gas retrieval algorithm for the infrared atmospheric sounding interferometer. J. Geophys. Res. 109, D21301, doi:10.1029/2004JD004821, 2004.